Optics and Laser Technology 131 (2020) 106454

Contents lists available at ScienceDirect

Optics and Laser Technology

journal homepage: www.elsevier.com/locate/optlastec

Full length article

Fabrication of nanocages on nickel using femtosecond laser ablation and trace level detection of malachite green and Nile blue dyes using surface enhanced Raman spectroscopic technique

Byram Chandu[a], Moram Sree Satya Bharati[a], Paweł Albrycht[b], Soma Venugopal Rao[a,*]

[a] Advanced Centre of Research in High Energy Materials (ACRHEM), University of Hyderabad, Hyderabad 500046, Telangana, India
[b] Institute of Physical Chemistry, Polish Academy of Sciences, Kasprzaka 44/52, 01-224 Warsaw, Poland

HIGHLIGHTS

- Periodic/ripple-like structures on Nickel fabricated using fs ablation in DW.
- 3D-like (groove) features Ni substrates were obtained in acetone.
- Ni periodic/3D-like structures were gold plated using thermal evaporation.
- SERS studies performed on MG and NB using these structures.
- Detection sensitives of 500 pM for MG and 5 nM for NB achieved.

ARTICLE INFO

Keywords:
Laser Induced Periodic Surface Structures (LIPSS)
Nanocages
Nickel Nanostructure (NS)
SERS
Malachite green
Nile blue

ABSTRACT

Over the last decade several research groups have accomplished the fabrication of 2D periodic and 3D nanocage like structures on different materials using diverse lithographic approaches. Herein, we present the detailed studies on the fabrication of femtosecond (fs) laser-induced periodic/ripple-like surface structures on nickel (Ni) substrate in distilled water whereas 3D-like (nanocages) features on Ni substrates in acetone by tailoring the laser processing parameters (pulse energy). The morphological studies of simultaneously obtained Ni nanoparticles (NPs)/nanostructures (NSs) in distilled water/acetone were meticulously studied using transmission electron microscope (TEM) and field emission scanning electron microscope (FESEM). The fabricated Ni periodic/3D-like structures were gold (Au) plated using thermal evaporation technique and subsequently utilized as surface enhanced Raman scattering (SERS) active sensors for detecting the traces of various analyte molecules such as malachite green (MG) and Nile blue (NB). The grooved Ni-Au substrates allowed us to detect extremely low concentrations of MG (500 pM) and NB (5 nM) and, significantly, utilizing a simple, portable Raman spectrometer. Moreover, the substrates have demonstrated superior reproducibility as well as multi-utility nature with a relative standard deviation (RSD) of < 17%. Additionally, Au- coated Ni grooved SERS substrates have demonstrated superior sensitivity and reproducibility in comparison to commercially available Ag-based SERS sensors (SERSitive, Poland). The proposed method of fabricating ripple and nanocages of Ni SERS platforms are highly viable to overcome the cost and one-time usage of substrates for on-site detection of several analyte molecules using a portable/hand-held Raman spectrometer.

1. Introduction

The generation of sub-wavelength surface structures on metals/dielectrics/polymers has been realized to be of importance to the advances in photonics and surface functionalization where the morphological features of such surfaces can effectually manipulate the mechanical [1] and optical [2] properties which are entirely different from those found in the bulk form. These surface structures have found enormous potential in a wide range of fields including catalysis [3], surface wetting (hydrophobicity and hydrophilicity) [4], sensing [5], and plasmonics [6]. Numerous nanofabrication techniques have been established to fabricate these subwavelength surface structures in which most regularly implemented methods are ion beam irradiation and electron beam lithography [7,8]. However, these techniques suffer

* Corresponding author.
E-mail address: soma_venu@uohyd.ac.in (S.V. Rao).

https://doi.org/10.1016/j.optlastec.2020.106454
Received 12 April 2020; Received in revised form 26 May 2020; Accepted 21 June 2020

from high cost, multistage procedures, low throughput, and are often time-consuming. Compared to the above described lithographic techniques, ultrafast laser processing has been accepted as an efficient and alternative tool for designing micro and nano-structures over a large area on various solid substrates [9]. More importantly, ultrafast laser ablation offers two foremost advantages (over the long pulse ablation) (a) high-quality surface structures with the desired accuracy because of mitigated heat effected zones (b) a net reduction in the ablation threshold at identical laser processing conditions (wavelength and focusing geometry). Nowadays, ultrafast laser processing has been widely applied to produce diverse subwavelength structures comprising micro/nanoscale structures [10], conical [11], 3D and 2D micro/nano spikes [12], holes and craters, mounds [13], and laser induced periodic surface structures (LIPSS) [14], which can significantly improve the chemical, optical and biological properties of target material surface such as optical data storage [15], color display [2] and anticounterfeiting [16], etc. The laser induced micro/nanoscale surface structures find potential applications in numerous fields including perfect light absorption [17,18], antireflective surfaces [18,19], and enhanced wetting properties [4,18]. Very few studies have demonstrated the utility of ultrafast laser fabricated micro/nanoscale structures in surface enhanced Raman scattering (SERS) based detection of various analyte molecules including explosives [20–29]. Chang et al. have recently demonstrated the fabrication of grating-like nanostructures (NSs) and Ag nanoparticles in the aqueous solutions simultaneously using femtosecond (fs) laser processing and further studied the efficacy these substates in SERS based identification Rhodamine 6G (Rh6G) [30]. In another study by Eric et al. fabricated large area NSs on Si substrate by fs laser irradiation and demonstrated the SERS activity of Si NSs after deposition of Ag film [31].

Recently, Bharathi et al. achieved fs laser processed groove-like silicon NSs combined with Ag/Au nanoparticles for successful identification of various explosive molecules [32]. In our recent study we have demonstrated the SERS activity of Au coated Fe based periodic surface structures achieved by liquid assisted fs laser ablation [33]. In the present work, we demonstrate the fabrication of ripple/periodic and nanocage-like surface structures on the Ni substrates with fs laser pulses by changing the ambient liquid and laser processing conditions. We demonstrate that these laser-irradiated Ni NSs can be utilized for SERS studies after deposition of a tiny amount of Au. Our studies also illustrate the practicability to prepare low-cost substrates by reducing the noble metal (Ag, Au) quantity. We also demonstrate the efficacy of these SERS substrates by comparing with the commercial Ag-based substrates provided by SERSitive. We believe that this technique laser ablation in liquids (LAL) which is capable of producing large area (3 square inches or more) SERS substrates in a single experiment followed by simple thermal evaporation method is beneficial for preparing low-cost and versatile SERS substrates.

2. Experimental details

Nickel (Ni, 99.9% purity, Alfa-Aeser) substrate was cleaned in acetone and water in an ultra-sonication bath for 5 min prior to the ablation experiments. Laser ablation experiments on nickel (Ni) substrate were performed using a Ti: sapphire fs laser amplifier (LIBRA, M/s Coherent) providing nearly transform limited pulses of ~50 fs duration at 1 kHz repetition rate and 800 nm wavelength. The Ni substrate was submerged in 5 mL of distilled water (DW)/acetone in a glass cell and the liquid layer thickness above the Ni surface was ~6 mm. During the laser processing, Ni target was translated using the X-Y stages at a scan speed of 0.5 mm/s with adjacent line pitch of ~30 μm. The employed pulse energy was 50 μJ, and the total laser processed area was ~25 mm^2. The calculated laser fluence on the target surface was ~0.15 J/cm^2. Ripple-like/periodic structures in DW whereas 3D-like surface structures in case of acetone were noticed on the Ni surface with above-described processing conditions. Subsequently, we proceeded with the ablation experiments in acetone (only) by keeping the stage parameters (scan speed and line interval) constant and varying the input pulse energies [(i) 100 μJ (ii) 200 μJ and (iii) 300 μJ)]. The prepared Ni NSs and NPs in acetone at energies of 100 μJ, 200 μJ, and 300 μJ were designated as NiNS1, NiNS2, NiNS3, and NiNP1, NiNP2, NiNP3, respectively. The surface morphology of Ni NSs was characterized by field emission scanning electron microscope (FESEM, Carl Zeiss). The size and crystallinity of the Ni NPs were investigated by high-resolution transmission electron microscope (HRTEM, FEI Tecnai G2 S-Twin) by dropping the tiny drop of colloidal solution on carbon coated copper grid then dried at room temperature. The analyte molecules of malachite green (MG) (dissolved in methanol) and Nile blue (NB) (dissolved in methanol) were prepared in the form of a stock solution (1×10^{-1} M) and then diluted successively to achieve various lower concentrations (of 10^{-12} to 10^{-4} M). The achieved laser patterned Ni surfaces were gold (Au) coated with thermal evaporation technique with deposition rate of ~0.2 Å/sec (time of deposition was ~20 min). The substrate to sample holder distance was around 10 cm and the chamber pressure before the start of experiment was 10^{-6} mbar. For the SERS measurements, analyte molecule (Malachite Green or Nile Blue) solutions (10 μL) were dropped on the Au-coated laser patterned Ni surfaces and were allowed to dry at room temperature. This was followed by the acquisition of the Raman spectra using a portable Raman spectrometer (i-Raman plus, B&W Tek, USA) with a laser operating at 785 nm wavelength and using an integration time of 5 s. Typically 80–90 mW of laser power was used. The effective spot size of the laser beam on the SERS substrate was 85 μm. However, the samples were found to be intact and was confirmed from subsequent SERS studies. With an increase in the integration time the input power required was reduced and consistent SERS signals were obtained.

3. Results and discussions

3.1. TEM studies of Ni NPs

Fig. 1(a)–(f) illustrate the TEM and HRTEM images of Ni NPs obtained by laser ablation in acetone with the pulse energies of (i) 100 μJ, (ii) 200 μJ, and (iii) 300 μJ, respectively. Fig. 1(a), (c), and (e) show the fabricated NPs at different pulse energies and the insets represent their corresponding size histograms. The measured NPs mean sizes were 20.61 ± 6.98 nm, 12.04 ± 3.95 nm, and 10.14 ± 4.03 nm for NiNP1, NiNP2 and NiNP3, respectively. With increasing the pulse energy, the NPs mean diameters were observed to decrease which could be accredited to the fragmentation of larger NPs through their interaction with later laser pulses. It is obvious from the HRTEM images [Fig. 1(b), (d), and (f)] that the obtained Ni NPs in all the cases are found to be spherical and are surrounded with the carbon/graphite shells (highlighted with red color rectangular boxes). The formation of graphite shells could be elucidated briefly as follows. When the high-intensity laser pulses are focused on the Ni plate surface in acetone it results in the formation of high- pressure and high-temperature conditions.

Due to these extreme conditions the solvent molecules could have decomposed into carbon atoms. Subsequently, carbon atoms evaporate and cause nucleation at the NP surface in the plasma plume. This nucleation consequently leads to the formation of graphite-like nanoshells [34–36]. However, the exact formation mechanism of graphite-like shells is still not completely understood and needs more systematic investigations.

3.2. FESEM studies of Ni NSs

Fig. 2(a) and (b) data illustrate the different morphological features on the fs laser-treated Ni target using different liquids (water and acetone). The employed laser pulse energy and stage scanning conditions were the same. We observed ripple-like (periodic) surface

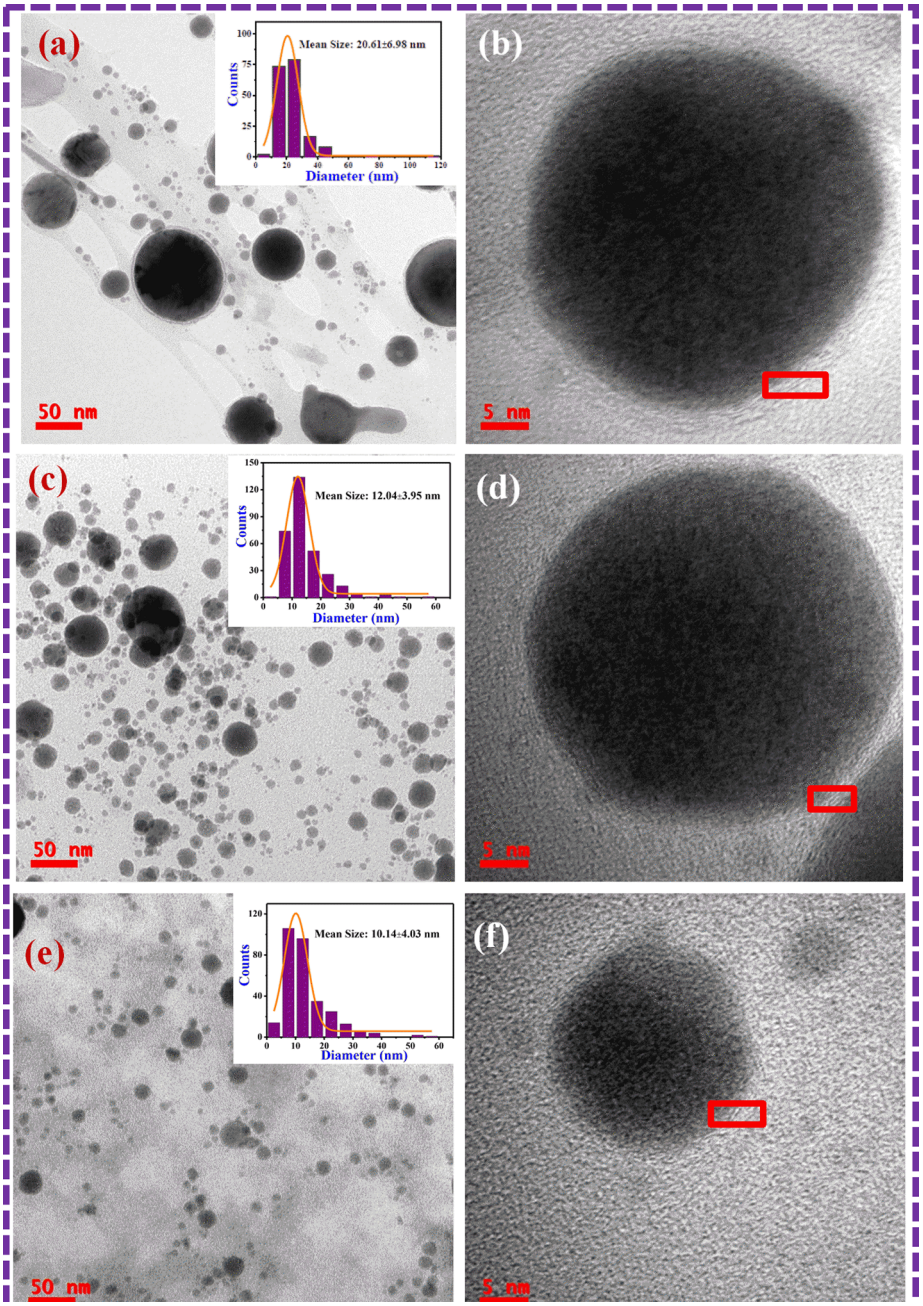

Fig. 1. TEM and HRTEM images of fs laser fabricated Ni NPs in acetone (a, b) NiNP1 (c, d) NiNP2 (e, f) NiNP3. Insets of figures (a), (c), and (e) illustrate their respective size histograms.

structures on the Ni surface with periods (Λ) in the 99–150 nm range when the irradiation was performed in water [shown in Fig. 2(a)]. We also noticed randomly distributed NPs in the gaps of periodic NS and their diameters were estimated to be in the 60–250 nm range [higher magnification FESEM image is shown in Fig. 2(a)]. The Ni NSs periodicities were found to be lower than the irradiated laser wavelength, which can again be termed as high spatial frequency LIPSS (HSFL) or subwavelength ripples. The formation mechanism of HSFL is still debated even though several theories have been presented earlier [18]. The orientation of HSFL ripples could be either parallel or perpendicular to the input laser polarization (HSFl ripples parallel to the laser polarization are shown with double arrow symbol in Fig. 2(a)). In earlier works, Albu et al. have demonstrated the formation of HSFL features with both orientations (parallel and perpendicular) using the fs laser irradiation of Ti in ethanol and water [37]. Also, they found that the spatial period of perpendicular oriented HSFL structures was smaller than the parallel oriented HSFL structures. A very recent report by Jalil et al. demonstrated the fabrication of subwavelength 2D ripple and conic structures on the Ni surface by temporally delayed fs laser pulses in ambient air [38]. Additionally, they described the control mechanism of the periodic/2D structures by adjusting the delays between three laser pulses and their formation mechanism was elucidated based on surface plasmon polariton interference model. Another recent study by Lim et al. demonstrated the manipulation of low spatial

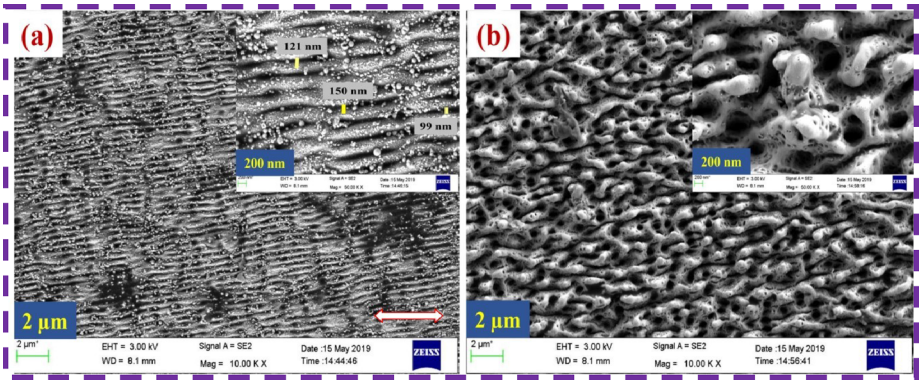

Fig. 2. FESEM images of fs laser fabricated Ni NSs in different liquids at pulse energy of 50 µJ (a) DW (b) acetone. Higher magnification images are illustrated in the insets of respective images. Double-headed arrow in figure (a) indicates the laser polarization direction.

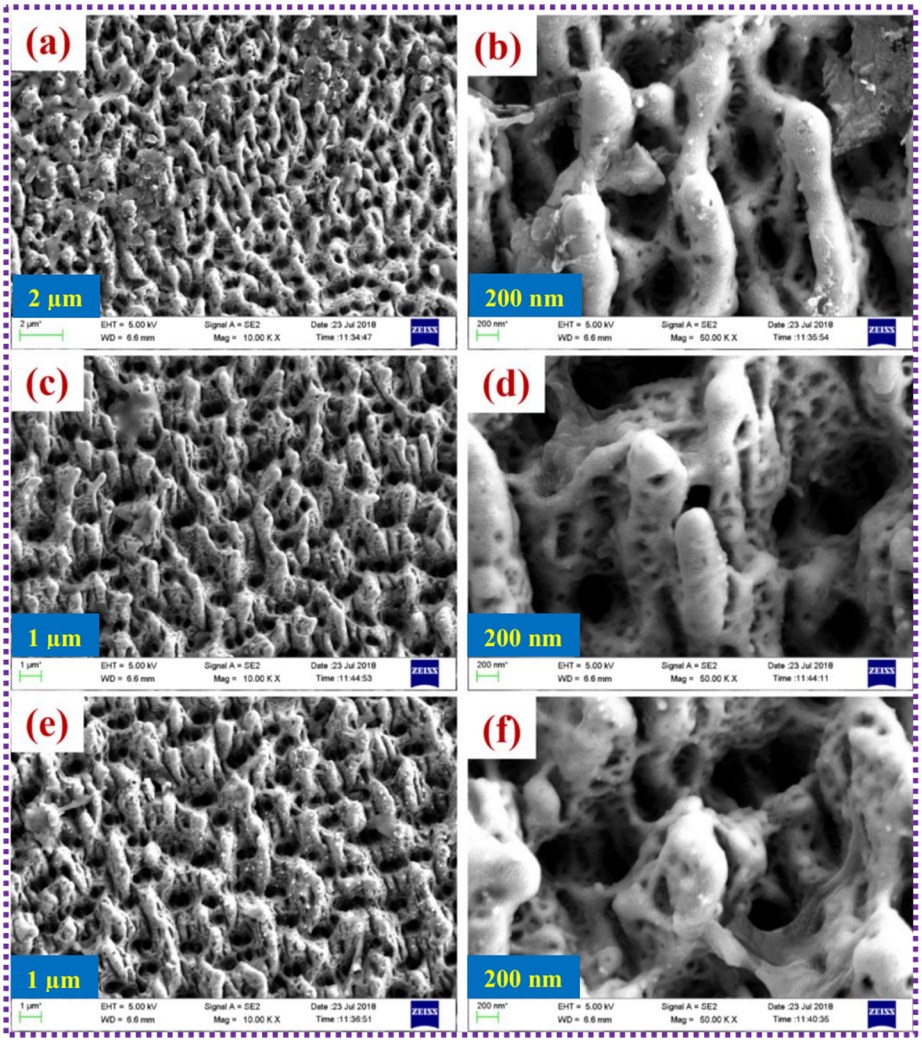

Fig. 3. Lower and higher magnification FESEM images of fs laser fabricated Ni NSs in acetone (a, b) NiNS1 (c, d) NiNS2 and (e, f) NiNS3.

frequency LIPSS (LSFL) features by irradiating the Ni target with fs pulses at different fluences, pulse numbers, and laser incident angles in the air environment [39].

However, in the present study, ripple and nanocages-like features were obtained by changing the ambient liquid. Interestingly, in the case of ablation in acetone nanocages (3D-like) surface features surrounded with nanoholes with diameters in the 250 nm–560 nm range were noticed. The discrepancy in the morphological features of the Ni surface is attributed to the effect of the surrounding liquid, which is evident from the FESEM images. Here, the liquid properties play a vital role in

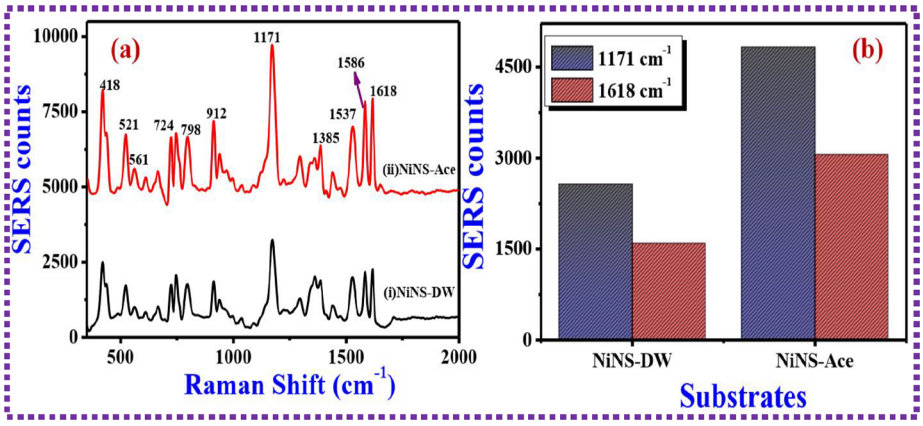

Fig. 4. (a) Recorded SERS signals from the Ni NSs for MG (5 nM) in (i) DW (black colored spectra, bottom) (ii) acetone (red colored spectra, top) (b) SERS signal intensity for the prominent MG peaks (at 1171 cm^{-1} and 1618 cm^{-1}) from the NiNS-DW and NiNS-Ace substrates. (For interpretation of the references to color in this figure legend, the reader is referred to the web version of this article.)

the observation of ripple/nanocages-like structures. Since the properties of DW and acetone are entirely different, they alter the cavitation bubble dynamics due to concurrent effects of the recoil pressure of the liquid media and induced surface tension forces [12,40,41]. Thus, nanostructures with different morphological features were obtained. We believe that these nanocages like features are more beneficial for SERS based detection than the ripple-like structures (described later in this section). Based on the observed results we further continued the fs laser irradiation experiments in acetone by varying the pulse energy. Fig. 3(a)-(f) depict the observed nanocages-like morphology under the pulse energy ranging from 100 μJ to 300 μJ at a scanning speed of 0.5 mm/s with a line to line spacing of 30 μm. From the magnified FESEM images in Fig. 3(b), (d) and (f), it can be understood that nanocages structure size, length and the diameter of surrounded nanoholes depends on the pulse energy. As the pulse energy increases, the height of nanocages increased from 0.3 μm to 1 μm, and the structures become uniform. At the pulse energy of 100 μJ, smaller size nanocages with irregular morphology were evident from the Fig. 3(a). With the rise of laser pulse energy, the laser-generated plasma could be further expanded and produces higher temperature, higher pressure and a shock wave at the nickel surface in the vicinity of confined liquid, consequently, the larger size and uniform nanocages are produced at higher pulse energy (300 μJ) [40].

3.3. SERS activity of Ni NSs prepared in DW and acetone

Before conducting the SERS measurements, thin Au film was coated on to the fs fabricated periodic Ni NSs using a thermal evaporation technique. The thickness of coated gold film on nickel substrate, measured using surface profilometer, was found to be ~20 nm. The SERS performance of both ripple-like (NiNS-DW) and nanocages (NiNS-Ace) structures of Ni substrate were evaluated with a probe analyte of MG (5 nM). In Fig. 4(a), curve (i) represents the SERS signals obtained from the ripple- like Ni structure, while curve (ii) indicates the spectra recorded from the nanocages structure of Ni substrate. In case of ripple structures, the large number of NPs observed over the laser patterned area may also contribute to the enhancement. However, this needs further detailed and separate investigations [33,42,43]. It is evident that the SERS signal intensity was superior for nanocages (NiNS-Ace) compared to the ripple-like (NiNS-DW) structure, and the data was illustrated in Fig. 4(b). The resulting high signal enhancement from the nanocages-like structures might be due to the generated high electromagnetic fields because of their sharp 3D-like (nanocages) features in comparison with the ripple-like features.

3.4. SERS activity of Ni NSs prepared in acetone at different pulse energies

The designed Ni NSs obtained using pulse energies of (i) 100 μJ (ii) 200 μJ and (iii) 300 μJ in acetone were labeled as NiNS1, NiNS2, and NiNS3, respectively. The SERS performance of Ni NSs was evaluated after Au plating (thickness ~20 nm) with a probe molecule of MG. Aliquot of MG (500 pM) solution was pipetted on to the fabricated Ni SERS substrates and allowed to dry. Subsequently, the SERS signals of MG were recorded from the as-fabricated Ni substrates. Fig. 5 presents the SERS signals of MG (500 pM) and were recorded from the Au coated NiNS1, NiNS2, and NiNS3 substrates. The characteristic Raman bands of MG were located at 418 cm^{-1}, 1171 cm^{-1}, 1378 cm^{-1}, and 1618 cm^{-1} and their peak assignments matched well with our earlier studies [25,33]. The following procedure was utilized to calculate the SERS enhancement factor (EF) [26,27,32].

$$EF = \frac{I_{SERS}}{I_{RAMAN}} \frac{C_{HC}}{C_{LC}}$$

where I_{SERS} is the integrated intensity of highly elevated Raman mode of probe molecule under consideration from the Au coated Ni nanostructured surface, and I_{RAMAN} is the integrated intensity of the same band obtained on plain Ni substrate. C_{HC} is the high concentration of probe molecule generating the normal Raman intensity from the Ni, and C_{LC} is the low concentration of probe molecule generating the Raman intensity from the Au coated Ni substrate. The obtained EFs for the prominent Raman bands of 1171 cm^{-1}, and 1618 cm^{-1} were 1.6×10^7, 1.5×10^7, 2.2×10^7, and 2.5×10^7, 2.4×10^7, and 3.25×10^7 for NiNS1, NiNS2 and NiNS3 substrates, respectively [as depicted in Fig. 5(b)]. Further, the SERS signals reproducibility was examined by collecting the Raman spectra at randomly selected fifteen (15) sites over the large area (5×5 mm^2) on each substrate and the data is shown with contour plot in Fig. 6(a)-(c). The relative slandered deviation (RSD) values were found to be ~11.7%, ~16.4%, and ~10.1% for the SERS intensity of MG (500 pM) at 1171 cm^{-1} peak and the spectra were obtained from the NiNS1, NiNS2 and NiNS3 substrates, respectively [depicted in Fig. 6(d)]. From obtained results it is evident that superior EFs and a good reproducibility was obtained for NiNS3 substrate. Furthermore, the detection sensitivity of NiNS3 substrate was further investigated by collecting the Raman signal of MG.

Fig. 7(a) and (b) illustrate the concentration dependent SERS spectra of MG (ranging from 50 nM to 50 pM) and the observed Raman modes were labelled in the inset. It is evident that the SERS intensity of the MG Raman bands gradually decreased with decreasing the MG concentration. The logarithm plot of the SERS intensity at 1171 cm^{-1} Raman mode depicted a linear dependence on the logarithm of the MG concentration [varied from 50 nM to 50 pM] and the obtained

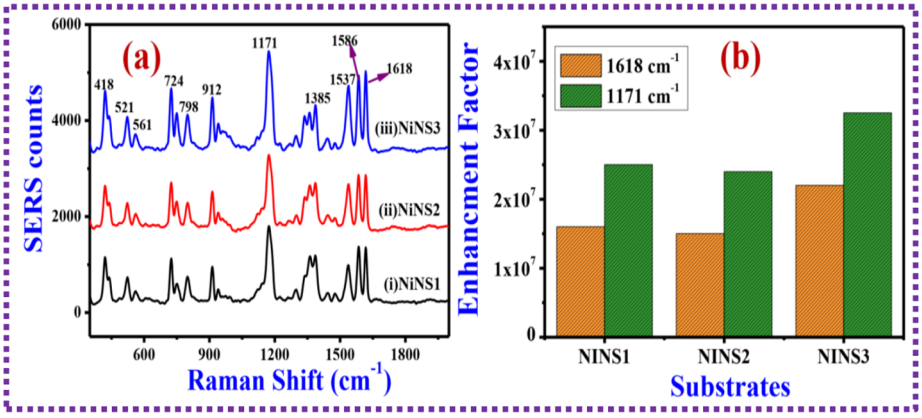

Fig. 5. SERS signals of MG (500 pM) recorded from the Au coated Ni NSs (i) NiNS1 (ii) NiNS2 and (iii) NiNS3. (b) Estimated enhancement factors by considering the major modes of MG dye (1618 cm^{-1} and 1171 cm^{-1}) from the NiNS1, NiNS2, and NiNS3 substrates.

correlation coefficient (R^2) was ~0.91 [Fig. 7(b)]. Several characteristic modes of MG are well-distinguishable even at the concentration of 50 pM, demonstrating the high sensitivity of NiNS3 substrate. Subsequently, the Ni substrates were re-used for the second time [after implementing appropriate cleaning procedures [20]] to detect another dye molecule Nile blue (NB). The normal Raman spectra of NB (5 mM) was obtained on plain Ni surface, as can be seen from the curve (i) in Fig. 8. The SERS spectra of NB (5 nM) recorded from the substrates of NiNS1, NiNS2, and NiNS3 was shown in Fig. 8. The NB prominent mode was located at 589 cm^{-1} is attributed to the C—C—C and C—N—C deformations [44]. The estimated EFs from the NiNS1, NiNS2, and NiNS3 were 5.9 × 10^5, 5.8 × 10^5, and 8.9 × 10^5, respectively. The Raman bands of NB observed from the SERS spectra (at higher concertation of NB) and their band assignments are presented Table 1.

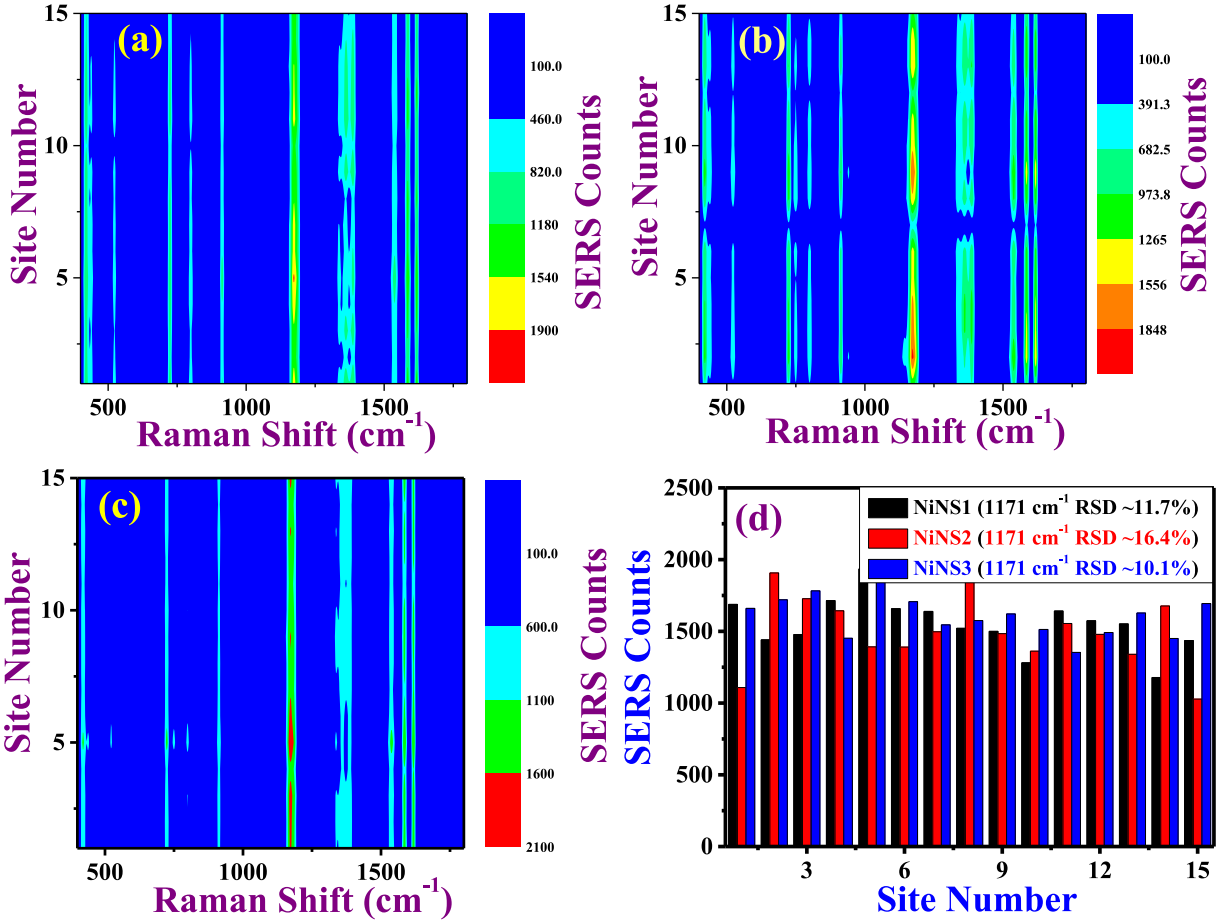

Fig. 6. Contour plot obtained from the 15 SERS spectra of MG (500 pM) recorded on (a) NiNS1 (b) NiNS2 and (c) NiNS3 substrates. (d) Histogram plot of SERS intensities for the prominent MG Raman band (1171 cm^{-1}) obtained from 15 spectra at different sites on NiNS1, NiNS2, and NiNS3 substrates.

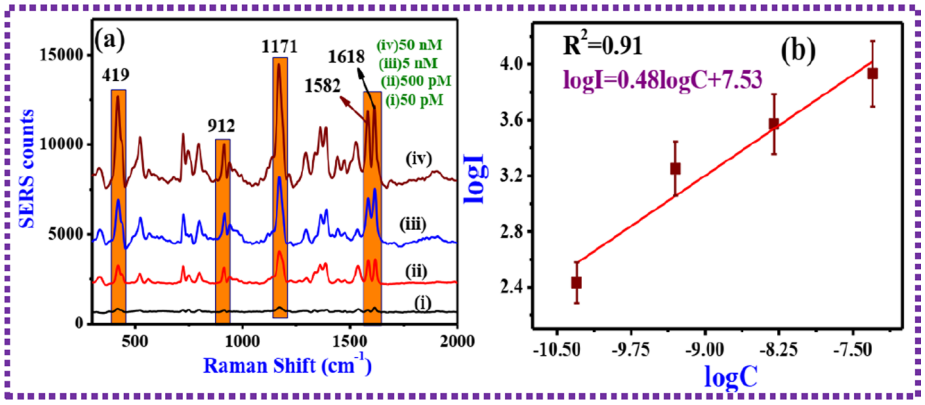

Fig. 7. (a) SERS signals of MG recorded at different concentrations [(i) 50 pM (ii) 500 pM (iii) 5 nM and (iv) 50 nM] recorded on NiNS3. (b) Log plot of MG SERS intensities at 1171 cm^{-1} mode against the different concentrations.

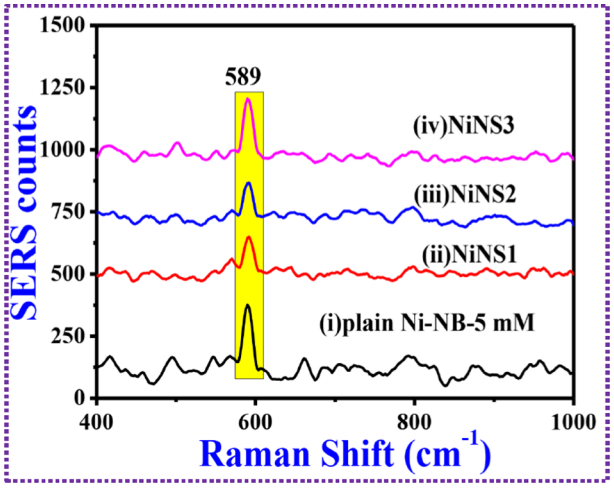

Fig. 8. Recorded Raman spectra of NB (5 mM) on (i) plain Ni surface. SERS spectra of NB (5 nM) recorded from (ii) NiNS1 (iii) NiNS2 and (iv) NiNS3 substrates.

3.5. SERS performance comparison with Ag-based commercial substrates

The performance of Au–plated Ni based SERS substrates are compared with a readily available commercial SERS (Ag-based) substrates, which are provided by SERSitive company [45]. These substrates were manufactured through the electrodeposition of Ag NPs on the ITO substrate with a dimension of 5 × 4 mm^2. Fig. 9(a) and (b) present the FESEM images of Ag-based commercial substrate acquired at lower and higher magnifications. The SERS performance of these substrates was verified by considering three probe molecules (i) picric acid (PA) (ii) MG and (iii) MB. Fig. 10(a) presents the SERS spectra of (i) PA (5 μM), (ii) MG (50 nM), and (iii) MB (5 nM). The obtained EF was ~6.3 × 10^6 for the main characteristic peak of MB 1620 cm^{-1}, for MG 1614 cm^{-1} peak ~4.5 × 10^5, and PA 820 cm^{-1} peak ~3.8 × 10^4. The intensity histogram demonstrating the reproducibility of the substrate with RSD ~14% for MB, ~26.17% for MG, and ~13.38% for PA, as shown in Fig. 10(b), (c) and (d). In the present study, the SERS performance of commercial substrates were also evaluated by detecting PA to compare with results obtained from our previous studies [26,32,33]. The detection sensitivity of Ag-based substrates is found to be comparable to our SERS substrates reported earlier [25,26,32]. Interestingly, the commercially obtained SERS substrates were in transit for a period of 3–4 weeks and this possibly could have affected their performance. Additionally, the commercial substrates had Ag while ours were Au-coated. With 785 nm excitation Au is expected to display stronger performance when compared to Ag. This could be one of the possible reasons for observing superior enhancement factors in our case. Detailed SERS studies with similar plasmonic metal will clearly identify the best among both. Furthermore, it is pertinent to note that that the presented results are obtained on only a few commercially available substrates and that our intention is not their rating or evaluation, but rather the presentation of the initial results.

The obtained EFs by our substrates (Au plated Ni) were in the range of 10^5-10^7 with superior reproducibility in the SERS signals (RSD < 17%). The presented results demonstrate the SERS performance of Ni based substrates are at least on par with the Ag-based commercial substrates (EFs of ~10^5–10^7, RSD < 17%). We believe there is a huge scope for optimizing and functionalizing these LIPSS [18,46] through the thorough understanding of their formation and apply them for the detection of various hazardous analyte molecules using the SERS technique.

Table 1
Nile Blue (NB) Raman modes (cm^{-1}) and their assignments [40].

S. No.	Reported Peaks (cm^{-1})	Observed peaks for NB (0.1 M)	Observed peaks in the SERS data	Peak Assignments
1	591	589	589	C–C–C and C–N–C deformations
2	664	662	662	In plane CCC deformation
3	1185	1172	1172	C–H bending
5	1491	1496	1496	C–C stretching
6	1643	1641	1641	Ring stretching

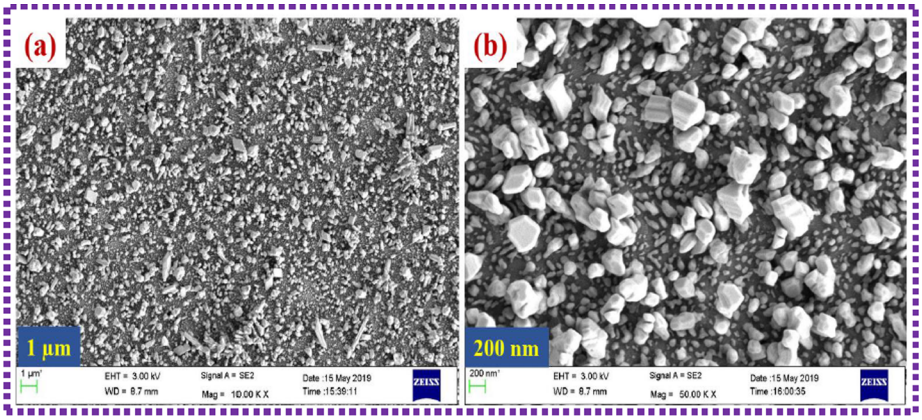

Fig. 9. FESEM images of the commercial substrate (SERSitive, Poland) at a (a) lower magnification and (b) higher magnification.

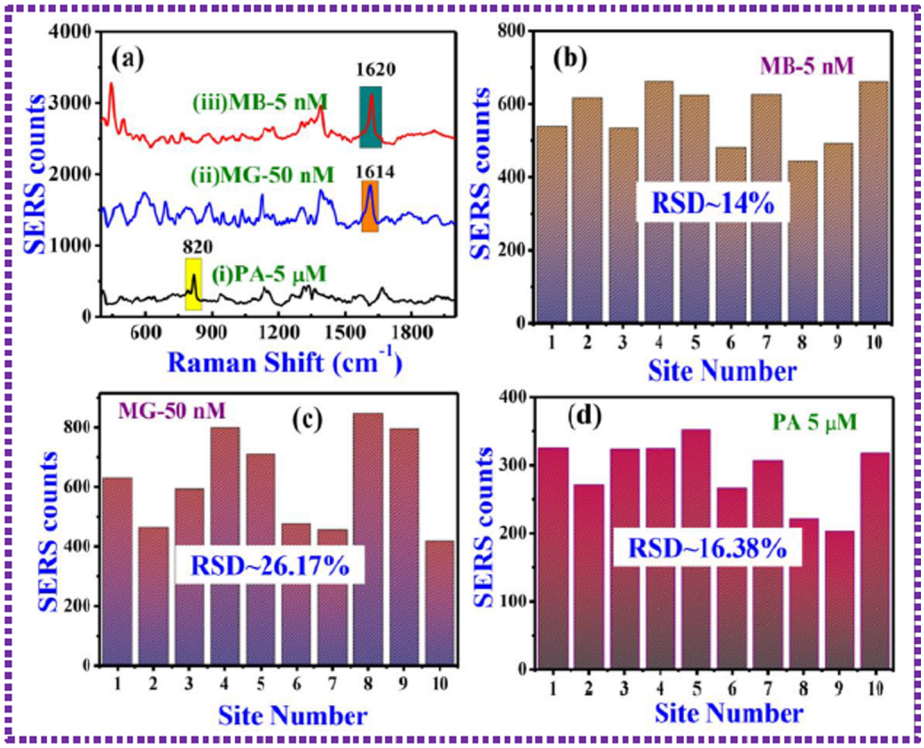

Fig. 10. (a) SERS spectra recorded from the commercial substrates (i) PA-5 µM (ii) MG-50 nM (iii) MB-5 nM. Histogram plot of SERS intensities for the prominent mode of each molecule (b) MB (1620 cm^{-1}) (c) MG (1614 cm^{-1}) and (d) PA (820 cm^{-1}) obtained from 10 spectra at different sites on commercial substrate.

4. Conclusions

Femtosecond laser texturing on Ni in DW and acetone was performed and detailed investigations were conducted to explore the morphological changes and their applications in SERS studies. In the case of DW, periodic surface structures were observed whereas 3D-like nanocages were observed on Ni surface in the presence of acetone. Hybrid Ni SERS substrates were achieved by simply depositing a thin layer of gold and subsequently these substrates were utilized for detecting very low concentrations of two analyte molecules, MG (500 pM) and NB (5 nM). The gold coated 3D-like nano features of Ni has demonstrated an increased detection sensitivity when compared to the periodic surface structures with EFs of $\sim 10^7$. Additionally, Au-coated Ni based SERS substrates have exhibited superior sensitivity (up to pM concentration detection) with good reproducibility in comparison to the commercial Ag-based SERS substrates (wherein we could detect only nM concentration analytes). These structures are cost-effective and scalable thereby presenting an opportunity to fabricate large-area SERS substrates.

CRediT authorship contribution statement

Byram Chandu: Investigation, Formal analysis, Software, Validation, Writing - original draft. **Moram Sree Satya Bharati:** Investigation, Formal analysis, Writing - original draft. **Paweł Albrycht:** Resources, Formal analysis, Writing - original draft, Writing - review & editing. **Soma Venugopal Rao:** Conceptualization, Methodology, Validation, Formal analysis, Resources, Writing - review & editing, Supervision, Project administration, Funding acquisition.

Declaration of Competing Interest

The authors declare that they have no known competing financial interests or personal relationships that could have appeared to influence the work reported in this paper.

Acknowledgement

DRDO, India for continuous financial support through Project #ERIP/ER/1501138/M/01/319/D (R&D) dated 27.02.2017.

References

[1] A.Y. Vorobyev, C. Guo, Laser makes silicon superwicking, Opt. Photonics News 21 (12) (2010) 38–38.
[2] A.Y. Vorobyev, C. Guo, Colorizing metals with femtosecond laser pulses, Appl. Phys. Lett. 92 (4) (2008) 041914.
[3] V. Berube, G. Radtke, M. Dresselhaus, G. Chen, Size effects on the hydrogen storage properties of nanostructured metal hydrides: A review, Int. J. Energy Res. 31 (6–7) (2007) 637–663.
[4] A.Y. Vorobyev, C. Guo, Direct femtosecond laser surface nano/microstructuring and its applications, Laser Photon. Rev. 7 (3) (2013) 385–407.
[5] U. Yogeswaran, S.-M. Chen, A review on the electrochemical sensors and biosensors composed of nanowires as sensing material, Sensors 8 (1) (2008) 290–313.
[6] D. Gramotnev, S. Bozhevolnyi, Plasmonics beyond the Diffraction Limit, Nat. Photonics 4 (2010) 83–91.
[7] F. Watt, A. Bettiol, J. Van Kan, E. Teo, M. Breese, Ion beam lithography and nanofabrication: a review, Int. J. Nanosci. 4 (03) (2005) 269–286.
[8] M. Altissimo, E-beam lithography for micro-/nanofabrication, Biomicrofluidics 4 (2) (2010) 026503.
[9] K. Ahmmed, C. Grambow, A.-M. Kietzig, Fabrication of micro/nano structures on metals by femtosecond laser micromachining, Micromachines 5 (4) (2014) 1219–1253.
[10] H. Huo, M. Shen, Platinum nanostructures formed by femtosecond laser irradiation in water, J. Appl. Phys. 112 (10) (2012) 104314.
[11] T. Yong Hwang, C. Guo, Polarization and angular effects of femtosecond laser-induced conical microstructures on Ni, J. Appl. Phys. 111 (8) (2012) 083518.
[12] E. Stratakis, Nanomaterials by ultrafast laser processing of surfaces, Sci. Adv. Mater. 4 (3–4) (2012) 407–431.
[13] C.A. Zuhlke, T.P. Anderson, D.R. Alexander, Fundamentals of layered nanoparticle covered pyramidal structures formed on nickel during femtosecond laser surface interactions, Appl. Surf. Sci. 283 (2013) 648–653.
[14] I. Gnilitskyi, T.-J.-Y. Derrien, Y. Levy, N.M. Bulgakova, T. Mocek, L. Orazi, High-speed manufacturing of highly regular femtosecond laser-induced periodic surface structures: physical origin of regularity, Sci. Rep. 7 (1) (2017) 1–11.
[15] J. Yao, C. Zhang, H. Liu, Q. Dai, L. Wu, S. Lan, A.V. Gopal, V.A. Trofimov, T.M. Lysak, Selective appearance of several laser-induced periodic surface structure patterns on a metal surface using structural colors produced by femtosecond laser pulses, Appl. Surf. Sci. 258 (19) (2012) 7625–7632.
[16] B. Dusser, Z. Sagan, H. Soder, N. Faure, J.-P. Colombier, M. Jourlin, E. Audouard, Controlled nanostructrures formation by ultra fast laser pulses for color marking, Opt. Express 18 (3) (2010) 2913–2924.
[17] A. Vorobyev, C. Guo, Enhanced absorptance of gold following multipulse femtosecond laser ablation, Phys. Rev. B 72 (19) (2005) 195422.
[18] C. Florian, S.V. Kirner, J. Krüger, J. Bonse, Surface functionalization by laser-induced periodic surface structures, J. Laser Appl. 32 (2) (2020) 022063.
[19] A. Vorobyev, C. Guo, Antireflection effect of femtosecond laser-induced periodic surface structures on silicon, Opt. Express 19 (105) (2011) A1031–A1036.
[20] S. Hamad, G.K. Podagatlapalli, M.A. Mohiddon, V.R. Soma, Cost effective nanostructured copper substrates prepared with ultrafast laser pulses for explosives detection using surface enhanced Raman scattering, Appl. Phys. Lett. 104 (26) (2014) 263104.
[21] S.V. Rao, G.K. Podagatlapalli, S. Hamad, Ultrafast laser ablation in liquids for nanomaterials and applications, J. Nanosci. Nanotechnol. 14 (2) (2014) 1364–1388.
[22] G.K. Podagatlapalli, S. Hamad, S.V. Rao, Trace-level detection of secondary explosives using hybrid silver–gold nanoparticles and nanostructures achieved with femtosecond laser ablation, J. Phys. Chem. C 119 (29) (2015) 16972–16983.
[23] G. Krishna Podagatlapalli, S. Hamad, S.P. Tewari, S. Sreedhar, M.D. Prasad, S. Venugopal Rao, Silver nano-entities through ultrafast double ablation in aqueous media for surface enhanced Raman scattering and photonics applications, J. Appl. Phys. 113 (7) (2013) 073106.
[24] G.K. Podagatlapalli, S. Hamad, M.A. Mohiddon, S.V. Rao, Effect of oblique incidence on silver nanomaterials fabricated in water via ultrafast laser ablation for photonics and explosives detection, Appl. Surf. Sci. 303 (2014) 217–232.
[25] C. Byram, S.S.B. Moram, V.R. Soma, SERS based detection of multiple analytes from dye/explosive mixtures using picosecond laser fabricated gold nanoparticles and nanostructures, Analyst 144 (7) (2019) 2327–2336.
[26] C. Byram, S.S.B. Moram, A.K. Shaik, V.R. Soma, Versatile gold based SERS substrates fabricated by ultrafast laser ablation for sensing picric acid and ammonium nitrate, Chem. Phys. Lett. 685 (2017) 103–107.
[27] C. Byram, V.R. Soma, 2, 4-dinitrotoluene detected using portable Raman spectrometer and femtosecond laser fabricated Au–Ag nanoparticles and nanostructures, Nano-Struct Nano-Objects 12 (2017) 121–129.
[28] K. Xu, C. Zhang, R. Zhou, R. Ji, M. Hong, Hybrid micro/nano-structure formation by angular laser texturing of Si surface for surface enhanced Raman scattering, Opt. Express 24 (10) (2016) 10352–10358.
[29] S. Hamad, S.S. Bharati Moram, B. Yendeti, G.K. Podagatlapalli, S. Nageswara Rao, A.P. Pathak, M.A. Mohiddon, V.R. Soma, Femtosecond laser-induced, nanoparticle-embedded periodic surface structures on crystalline silicon for reproducible and multi-utility SERS platforms, ACS Omega 3 (12) (2018) 18420–18432.
[30] H.-W. Chang, Y.-C. Tsai, C.-W. Cheng, C.-Y. Lin, Y.-W. Lin, T.-M. Wu, Nanostructured Ag surface fabricated by femtosecond laser for surface-enhanced Raman scattering, J. Colloid Interface Sci. 360 (1) (2011) 305–308.
[31] E.D. Diebold, N.H. Mack, S.K. Doorn, E. Mazur, Femtosecond laser-nanostructured substrates for surface-enhanced Raman scattering, Langmuir 25 (3) (2009) 1790–1794.
[32] S.S.B. Moram, A.K. Shaik, C. Byram, S. Hamad, V.R. Soma, Instantaneous trace detection of nitro-explosives and mixtures with nanotextured silicon decorated with Ag–Au alloy nanoparticles using the SERS technique, Anal. Chim. Acta 1101 (2020) 157–168.
[33] C. Byram, S.S.B. Moram, V.R. Soma, Surface-enhanced Raman scattering studies of gold-coated ripple-like nanostructures on iron substrate achieved by femtosecond laser irradiation in water, J. Raman Spectrosc. 50 (8) (2019) 1103–1113.
[34] H.J. Jung, M.Y. Choi, Specific solvent produces specific phase Ni nanoparticles: a pulsed laser ablation in solvents, J. Phys. Chem. C 118 (26) (2014) 14647–14654.
[35] Z. Abdullaeva, E. Omurzak, C. Iwamoto, H.S. Ganapathy, S. Sulaimankulova, C. Liliang, T. Mashimo, Onion-like carbon-encapsulated Co, Ni, and Fe magnetic nanoparticles with low cytotoxicity synthesized by a pulsed plasma in a liquid, Carbon 50 (5) (2012) 1776–1785.
[36] H. Zhang, C. Liang, J. Liu, Z. Tian, G. Shao, The formation of onion-like carbon-encapsulated cobalt carbide core/shell nanoparticles by the laser ablation of metallic cobalt in acetone, Carbon 55 (2013) 108–115.
[37] C. Albu, A. Dinescu, M. Filipescu, M. Ulmeanu, M. Zamfirescu, Periodical structures induced by femtosecond laser on metals in air and liquid environments, Appl. Surf. Sci. 278 (2013) 347–351.
[38] S.A. Jalil, J. Yang, M. Elkabbash, Y. Lei, W. He, C. Guo, Formation of uniform two-dimensional subwavelength structures by delayed triple femtosecond laser pulse irradiation, Opt. Lett. 44 (9) (2019) 2278–2281.
[39] H.U. Lim, J. Kang, C. Guo, T.Y. Hwang, Manipulation of multiple periodic surface structures on metals induced by femtosecond lasers, Appl. Surf. Sci. 454 (2018) 327–333.
[40] G. Li, J. Li, C. Zhang, Y. Hu, X. Li, J. Chu, W. Huang, D. Wu, Large-area one-step assembly of three-dimensional porous metal micro/nanocages by ethanol-assisted femtosecond laser irradiation for enhanced antireflection and hydrophobicity, ACS Appl. Mater. Interfaces 7 (1) (2015) 383–390.
[41] A. De Bonis, T. Lovaglio, A. Galasso, A. Santagata, R. Teghil, Iron and iron oxide nanoparticles obtained by ultra-short laser ablation in liquid, Appl. Surf. Sci. 353 (2015) 433–438.
[42] Y. Kalachyova, D. Mares, V. Jerabek, K. Zaruba, P. Ulbrich, L. Lapcak, V. Svorcik, O. Lyutakov, The effect of silver grating and nanoparticles grafting for LSP–SPP coupling and SERS response intensification, J. Phys. Chem. C 120 (19) (2016) 10569–10577.
[43] Y. Kalachyova, D. Mares, V. Jerabek, P. Ulbrich, L. Lapcak, V. Svorcik, O. Lyutakov, Ultrasensitive and reproducible SERS platform of coupled Ag grating with multi-branched Au nanoparticles, Phy. Chem. Chem. Phy 19 (22) (2017) 14761–14769.
[44] F. Xu, H. Lai, H. Xu, Gold nanocone arrays directly grown on nickel foam for improved SERS detection of aromatic dyes, Anal. Methods 10 (26) (2018) 3170–3177.
[45] https://www.sersitive.eu/.
[46] I.N. Saraeva, S.I. Kudryashov, A.A. Rudenko, M.I. Zhilnikova, D.S. Ivanov, D.A. Zayarny, A.V. Simakin, A.A. Ionin, M.E. Garcia, Effect of fs/ps laser pulsewidth on ablation of metals and silicon in air and liquids, and on their nanoparticle yields, Appl. Surf. Sci. 470 (2019) 1018–1034.